2026 IEEE International Conference on Robotics and Automation (ICRA 2026)
June 1-5, 2026. Vienna, Austria

Singularity Analysis of ABB's GoFa 5 Robot Arm

Axel Refalo[1], Ilian Bonev[1], and Clément Gosselin[2]

***Abstract*— In the past decade, manipulator arms with non-traditional architectures—once found mainly in space and painting applications—have become popular as collaborative robots. Examples include ABB's YuMi and GoFa, Kinova's Link 6, and Fanuc's CRX. These cobots lack closed-form inverse kinematics solutions, making it impossible to unambiguously select one configuration among the 16 (or infinitely many) that correspond to a given end-effector pose, which may create safety risks. Moreover, they exhibit far more singularities than typical manipulators, and most of them are far more complex to describe. Nevertheless, many authors argue these manipulators can provide improved dexterity and a larger workspace. In this paper, we analyze the singularities of ABB's GoFa using Grassmann line geometry and provide straightforward, sufficient (though conservative) conditions for avoiding them. Then, while GoFa can exhibit over a dozen distinct singularities compared to only three (wrist, shoulder, and elbow) for traditional robot arms, we attempt to quantify which architecture actually possesses a greater amount of singular and near-singular configurations.**

I. Introduction

Kinematic singularities are inherent to the control of mechanisms. They correspond to configurations in which the velocity model becomes indeterminate [1]. In industrial robot arms, these singularities pose significant challenges: they typically cause the robot to stop when operating in Cartesian mode and are difficult to predict by inspection.

If robotic cells were designed and programmed using optimization-based or learning-based planners, singularities could often be avoided automatically (e.g., [2]–[4]). However, in practice, most applications are implemented through trial and error, even when using offline programming and simulation software. It is therefore essential for robot programmers and cell designers to understand what causes a robot configuration to be singular, and how to avoid it.

Early on, Pieper [5] showed that when a 6-DOF (degree of freedom) robot arm has three consecutive revolute (R) joints with concurrent (e.g. Fig. 1a) or parallel axes (e.g. Fig. 1b), its inverse kinematics (IK) admits a closed-form solution and its singularities can be easily described. Recently, counter examples to Pieper's criteria were shown and novel 6R designs with closed-form IK were presented [6]. Other 6R robots lack analytic IK: one ends up with a degree-16 univariate polynomial [7], or with geometric formulations that nevertheless require numerical root finding [8].

Thus, it is not surprising that, since the 1970s, the vast majority of 6-DOF industrial robots have retained spherical wrists [9] (see Fig. 1a). A common exception is painting robots, which are often taught and executed in joint mode, so the complex inverse kinematics and singularity loci are less visible in routine operation. Since 2008, Universal Robots has popularized 6R arms with three consecutive parallel axes and contributed to the emergence of collaborative robots (cobots). The singularities of UR cobots (Fig. 1b) are comparable to those of spherical-wrist manipulators [10].

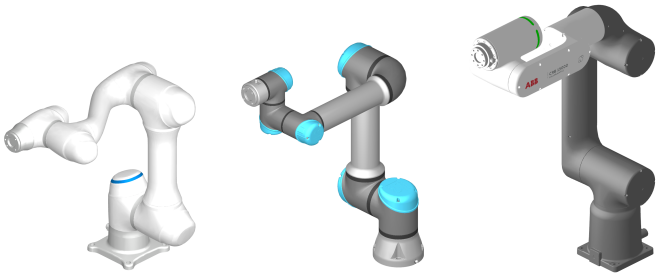

(a) Doosan's A0509 (b) UR's UR5e (c) ABB's GoFa 5

Fig. 1: Three distinct robot arm architectures

In the past decade, the rise of cobots, which are intended to be easier to use, has paradoxically reintroduced architectures with complex kinematics. The first was ABB's YuMi, a 7R cobot with no consecutive intersecting axes, which was recently shown to have very intricate singularities [11]. A 6R cobot with complex singularities, Kinova's Link 6, was studied in [12]. Fanuc's CRX and ROKAE's xMate cobot series are yet another example. This paper addresses the study of singularities of another popular 6R cobot series that does not respect Pieper's principle: ABB's GoFa (Fig. 1c).

One major problem with such cobots is that there is no way to unambiguously label one configuration among the 16 possible, unlike traditional 6R robots, where three binary parameters (shoulder, elbow, wrist) allow selecting among the 8 configurations. Worse still, in GoFa, for example, although all 16 inverse kinematic solutions can be feasible, the controller somehow allows only 8 of them. Thus, if an end-effector pose is "taught" in one of the prohibited solutions, the robot will return to that pose in a different configuration, which can be dangerous. These cobots are also cuspidal (see [3] and [13]), causing similar safety issues.

Needless to say, such complex singularities and behaviors are not documented in detail in the manufacturer's user guides. The first objective of this paper is therefore to describe the singularities of GoFa and, given their complexity, to provide straightforward sufficient (though conservative) conditions for avoiding them. It is also worth questioning whether the deviation from Pieper's condition is justified given the resulting complexity. A second objective of this

This work was funded by the Fonds de Recherche du Québec, Nature et Technologie (FRQNT).

[1]A. Refalo and I. Bonev are with the École de Technologie Supérieure, Montréal, QC, Canada ilian.bonev@etsmtl.ca

[2]C. Gosselin is with the Université Laval, Québec, QC, Canada

paper is therefore to quantify which of the three architectures shown in Fig. 1 exhibits a greater amount of singular and near-singular robot positions.

In the next section, we briefly present the methodology used. Then in Section III, we describe the kinematics of GoFa, and provide its Jacobian matrix and its determinant. Next, in Section IV, we classify and describe all unique singularities present in GoFa. In Section V, we attempt to compare GoFa with other simpler designs, in terms of singularities. Conclusions are given in Section VI.

II. Methodology

Mathematically, a manipulator is said to be in a singularity when its Jacobian matrix is not invertible [14]—i.e., when it is rank-deficient. This results in the loss of at least one DOF in velocity and a corresponding ability to resist arbitrary external wrenches along the affected directions without requiring any joint torque [15]. Such configurations are often challenging to characterize geometrically for practitioners.

Extensive research has been devoted to analyzing the singularities of robot manipulators as detailed in [11] and [12]. In this work, we use the methodology proposed in [12], to characterize and analyze singularities and to map them in the joint space. Namely, we use Grassmann algebra (also known as exterior algebra) and the wedge product, which has proven effective in singularity analysis [16], [17]. These tools enable the derivation of both algebraic and geometric conditions under which a singularity occurs.

In contrast to [12], where singularities are merely described, we go one step further and provide straightforward, sufficient (though conservative) conditions for avoiding them. This strategy is cleverly used by ABB in the actual YuMi robot [11], but has not yet been applied to the GoFa.

Then, in an attempt to compare GoFa with conventional cobots architectures, we also describe the structure of the singularities in the joint space—a representation rarely explored in the literature [18]. Finally, we compare the manipulability of all designs throughout a given Cartesian workspace.

III. Jacobian matrix of ABB's GoFa

ABB's GoFa series (CRB 15000) consists of three different models—GoFa 5, 10, and 12—with a few unique singularities each. We will focus mainly on the GoFa 5 (Fig. 1c), but will provide remarks for the other two models. In all three models, the only deviation from the popular spherical-wrist design is the offset between axes 5 and 6.

To model the kinematics of ABB's GoFa 5, we use the *distal variant of the Denavit–Hartenberg convention* in which the homogeneous matrix representing the pose of reference frame i with respect to reference frame $i-1$ is

$$\begin{aligned}\mathbf{H}_i^{i-1} &= \mathrm{rot}_{z_{i-1}}(\theta_i)\,\mathrm{trans}_{z_{i-1}}(d_i)\,\mathrm{trans}_{x_i}(a_i)\,\mathrm{rot}_{x_i}(\alpha_i)\\ &= \begin{bmatrix} c_{\theta_i} & -s_{\theta_i}c_{\alpha_i} & s_{\theta_i}s_{\alpha_i} & a_i c_{\theta_i} \\ s_{\theta_i} & c_{\theta_i}c_{\alpha_i} & -c_{\theta_i}s_{\alpha_i} & a_i s_{\theta_i} \\ 0 & s_{\alpha_i} & c_{\alpha_i} & d_i \\ 0 & 0 & 0 & 1 \end{bmatrix}, \end{aligned} \tag{1}$$

where $c_{\theta_i} = \cos\theta_i$, $s_{\theta_i} = \sin\theta_i$, etc.

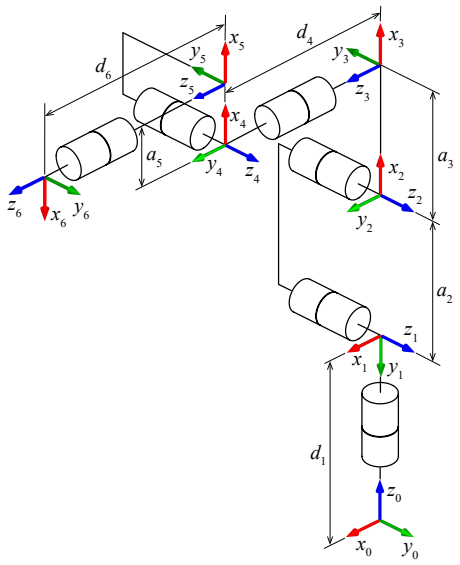

Fig. 2: The schematic of ABB's GoFa 5 (and GoFa 12) with its DH parameters and frames (all joint angles are zero)

The schematic of the robot with its DH reference frames is given in Fig. 2, while the numeric values of all DH parameters are listed in Table I. In GoFa 10, there is also an offset between the axes of joints 1 and 2.

TABLE I: DH parameters of ABB's GoFa 5

i	θ_i	d_i (mm)	a_i (mm)	α_i
1	θ_1	265	0	-90°
2	$\theta_2 - 90^\circ$	0	444	0°
3	θ_3	0	110	-90°
4	θ_4	470	0	90°
5	θ_5	0	80	-90°
6	$\theta_6 + 180^\circ$	101	0	0°

The Jacobian matrix of the robot can be defined as:

$$\mathbf{J} = \begin{bmatrix} \$_1 & \$_2 & \$_3 & \$_4 & \$_5 & \$_6 \end{bmatrix}, \tag{2}$$

where each column is a screw defined as

$$\$_i = \begin{bmatrix} \mathbf{e}_i \\ \mathbf{e}_i \times \mathbf{r}_i \end{bmatrix}. \tag{3}$$

In the above, $\mathbf{e}_i$ is the unit vector along the z_i axis and $\mathbf{r}_i$ represents the coordinates of the origin of frame i. In other words, $\mathbf{J}$ is with respect to the base origin [14]. If, in addition, we express these vectors in frame 4, the expression for $\mathbf{J}$ is more compact. Indeed, for GoFa 5, we obtain:

$$\mathbf{J} = \begin{bmatrix} c_{23} & 0 & 0 & 0 & s_4 & -c_4 s_5 \\ 0 & -1 & -1 & 0 & -c_4 & -s_4 s_5 \\ -s_{23} & 0 & 0 & 1 & 0 & c_5 \\ 0 & a_2 s_3 & 0 & 0 & d_4 c_4 & s_4(d_4 s_5 + a_5) \\ -a_3 s_{23} - a_2 s_2 & 0 & 0 & 0 & d_4 s_4 & -c_4(d_4 s_5 + a_5) \\ 0 & a_2 c_3 + a_3 & a_3 & 0 & 0 & 0 \end{bmatrix}, \tag{4}$$

where $s_1 = \sin\theta_1$, $c_1 = \cos\theta_1$, $s_{23} = \sin(\theta_2 + \theta_3)$, etc.

The determinant of the Jacobian can be easily obtained as:

$$\begin{aligned}\det(\mathbf{J}) = \\ a_2 s_2 \Big[& s_5 \big(a_2 a_3 s_3 + a_2 d_4 c_3 - 2 a_3 d_4 s_3^2 \\ & + a_3^2 (1 + c_3 s_3) - d_4^2 c_3 s_3 \big) \\ & + a_5 c_3 (a_2 s_4^2 + a_3 s_4^2 - a_3 s_3^2 - d_4 s_3) \Big] \\ + a_2 c_2 \Big[& s_5 (a_3 s_3 + d_4 c_3)^2 + a_5 s_3 c_3 (a_3 + d_4) \Big].\end{aligned} \tag{5}$$

The robot is at a singularity, when the above expression is zeroed. Unfortunately, although this expression is relatively simple, it cannot be factored or otherwise decomposed into simpler forms to identify all the unique singularity conditions. We must therefore use a different approach.

IV. Analyses of all singular configurations

Since the determinant of the Jacobian does not depend on θ_1 and θ_6, we restrict the search for singularities to a 4-dimensional (4D) subset of the joint space, denoted $\mathcal{Q}'$:

$$\det(\mathbf{J}(\mathbf{q}')) = 0, \quad \mathbf{q}' = (\theta_2, \theta_3, \theta_4, \theta_5) \in \mathcal{Q}'. \tag{6}$$

In GoFa 5, joints 2, 4, and 5 are restricted to $\pm 180°$, while joint 3 is bounded between $-225°$ and $85°$. Within these limits, self-collisions may occur; however, we ignore them when computing the exact fraction of $\mathcal{Q}'$ corresponding to each singularity type. To prevent double counting, the value $-180°$ is excluded from the ranges of joints 2, 4, and 5.

Searching for singularities in the complete 4D space $\mathcal{Q}'$ is computationally expensive. Instead, we use the wedge product from exterior algebra [19]. By computing the wedge product of two screws (i.e., two columns of the Jacobian), we can determine for which values of $\mathbf{q}'$ the resulting vector vanishes and the screws become dependent. In some cases, no value of $\mathbf{q}'$ zeros the wedge product, indicating that the screws are independent. This property can be extended to more than two screws and allows us to identify all groups of dependent screws and to derive the algebraic conditions under which the screws in a given group become dependent:

$$\$_i \wedge \cdots \wedge \$_j = 0 \quad \Leftrightarrow \quad \$_i, \cdots, \$_j \text{ are dependent} \tag{7}$$

For example, two dependent revolute screws imply that the corresponding joints instantaneously produce the same motion, so one joint contributes no additional degree of freedom. This occurs when the two joint axes coincide, making one of the revolute joints redundant since it no longer contributes additional mobility.

To simplify the problem and avoid an exhaustive search of $\mathcal{Q}'$, we first eliminate screw sets that are always independent. Following the approach of [11] and [12], we examine all combinations of screws and compute their wedge products to identify independencies. This requires evaluating all possible combinations of k screws, for k ranging from 2 to 6, which amounts to a total of $\sum_{k=2}^{6} \binom{6}{k} = 57$ wedge products. In our case, this analysis reveals that 47 of these sets are independent, leaving only 10 minimal sets of screws that can become dependent, described in Table II.

Some screw sets are obviously independent, such as $\$_1$ and $\$_2$. For the remaining sets, we use MATLAB's `GlobalSearch` nonlinear optimizer with multiple random starts to determine whether a given wedge product can converge to a global minimum, and return example joint configurations if found. To avoid redundancy in the detection of singular configurations, we define a constraint function involving all previously identified dependent screw sets, which must remain non-zero during the optimization or higher than a small tolerance ϵ (chosen empirically around 10^{-3}). The resulting optimization problem can be formulated as follows for a subset $i, \ldots, j$:

$$\begin{cases} \text{minimize}((\$_i \wedge \cdots \wedge \$_j)^2) \\ \text{with } (\$_k \wedge \cdots \wedge \$_l)^2 \times \cdots \times (\$_m \wedge \cdots \wedge \$_n)^2 > \epsilon \end{cases} \tag{8}$$

where the nested subsets $(\$_k, \ldots, \$_l), \ldots, (\$_m, \ldots, \$_n)$ have already been identified as dependent for certain values of $\mathbf{q}'$. For example, once it is established that $\$_1$ and $\$_6$ can be dependent, as well as $\$_1$ and $\$_4$, we seek $\mathbf{q}'$ in which $\$_1$, $\$_4$, and $\$_6$ are dependent, while no pair among them is.

The optimization performs well for any 6R robot, and iterating through all screw sets takes only a few minutes. The joint angles examples provided by the optimizer for each singularity are particularly useful, as they help pinpoint the geometric condition. As for the identification of the geometric conditions that correspond to each dependency, we refer to [20]. However, identifying the algebraic conditions associated with singularities requires further analysis by factoring the wedge products of the identified sets of potentially dependent screws.

Although the completeness of the geometric conditions cannot be formally proven, the presence of numerous near-singular configurations clustering around them suggests that no fundamental singularity has been overlooked.

The ten different sets of screws that can be dependent, i.e., the ten different singularities are presented in Table II, along with the corresponding geometric conditions and the form of the singularity manifold in $\mathcal{Q}'$ derived from the equations. The lengths and areas of these manifolds are estimated by discretizing them into line segments and square elements, respectively, and summing these elements.

For each of two of the subsets, there can be two slightly different geometric conditions: cases B_2 and B_2', and D_2 and D_2'. Thus, for each of the twelve singularity conditions, a numerical example of joint values is given in the last column of Table II, and the corresponding robot configuration is illustrated in the matching subfigure of Fig. 3.

In Table II and Fig. 3, $\mathcal{L}_i$ refers to the line that coincides with the axis of joint i. In the examples shown in Table II, the joint values that can be arbitrary are displayed in light gray. The values displayed in color are related to Table III, but will be explained later.

We proceed by analyzing the singularities in detail, starting with those associated with subsets of two screws and continuing with subsets of three, four, five, and finally six.

TABLE II: Singularities of GoFa 5

Case	Axes	Condition	Loci in $\mathcal{Q}'$, 4D space of joints 2–5	Examples of joint angles
A_1	$\mathcal{L}_1, \mathcal{L}_4$	$\mathcal{L}_1 \equiv \mathcal{L}_4$	2 planes, total area of 79 rad^2	$0°$, $14.34°$, $-104.34°$, $-10°$, $80°$, $0°$
A_2	$\mathcal{L}_1, \mathcal{L}_6$	$\mathcal{L}_1 \equiv \mathcal{L}_6$	4 curves, total length of 51 rad	$0°$, $-30°$, $-8.1°$, $0°$, $-51.9°$, $0°$
B_1	$\mathcal{L}_1, \mathcal{L}_4, \mathcal{L}_5$		2 surfaces, total area of 157 rad^2	$0°$, $-30°$, $-19.45°$, $-90°$, $-80°$, $0°$
B_2	$\mathcal{L}_1, \mathcal{L}_4, \mathcal{L}_6$		4 surfaces, total area of 297 rad^2	$0°$, $10°$, $10°$, $0°$, $-7.77°$, $0°$
B_2'	$\mathcal{L}_1, \mathcal{L}_4, \mathcal{L}_6$		8 lines, total length of 61 rad	$0°$, $40°$, $50°$, $0°$, $0°$, $0°$
B_3	$\mathcal{L}_2, \mathcal{L}_3, \mathcal{L}_5$		2 planes, total area of 79 rad^2	$0°$, $20°$, $-76.83°$, $0°$, $60°$, $0°$
B_4	$\mathcal{L}_2, \mathcal{L}_3, \mathcal{L}_6$		4 lines, total length of 25 rad	$0°$, $20°$, $-78.69°$, $90°$, $90°$, $0°$
C_1	$\mathcal{L}_1, \mathcal{L}_2, \mathcal{L}_4, \mathcal{L}_6$		2 planes, total area of 79 rad^2	$0°$, $20°$, $-104.34°$, $15°$, $-174.9°$, $0°$
D_1	$\mathcal{L}_1, \mathcal{L}_2, \mathcal{L}_3, \mathcal{L}_4, \mathcal{L}_5$	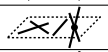	2 planes, total area of 79 rad^2	$0°$, $0°$, $-76.83°$, $15°$, $25°$, $0°$
D_2	$\mathcal{L}_1, \mathcal{L}_2, \mathcal{L}_3, \mathcal{L}_4, \mathcal{L}_6$	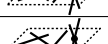	2 surfaces, total area of 199 rad^2	$0°$, $0°$, $40°$, $15°$, $-8.18°$, $0°$
D_2'	$\mathcal{L}_1, \mathcal{L}_2, \mathcal{L}_3, \mathcal{L}_4, \mathcal{L}_6$	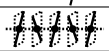	16 points	$0°$, $90°$, $0°$, $-90°$, $-9.8°$, $0°$
E_1	$\mathcal{L}_1, \mathcal{L}_2, \mathcal{L}_3, \mathcal{L}_4, \mathcal{L}_5, \mathcal{L}_6$	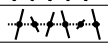	4 surfaces, total area of 397 rad^2	$0°$, $-30°$, $30°$, $-90°$, $-8.63°$, $0°$

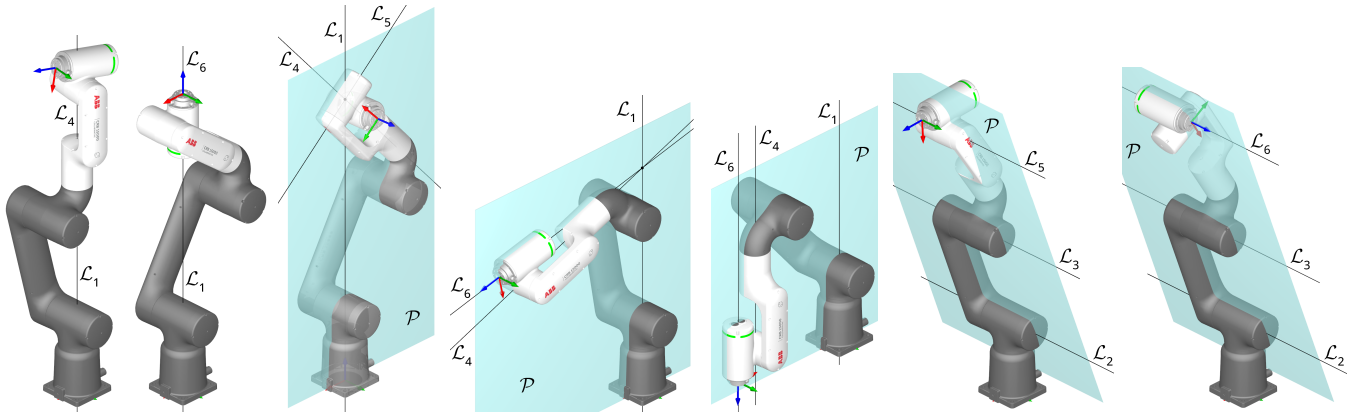

(a) case A_1 (b) case A_2 (c) case B_1 (d) case B_2 (e) case B_2' (f) case B_3 (g) case B_4

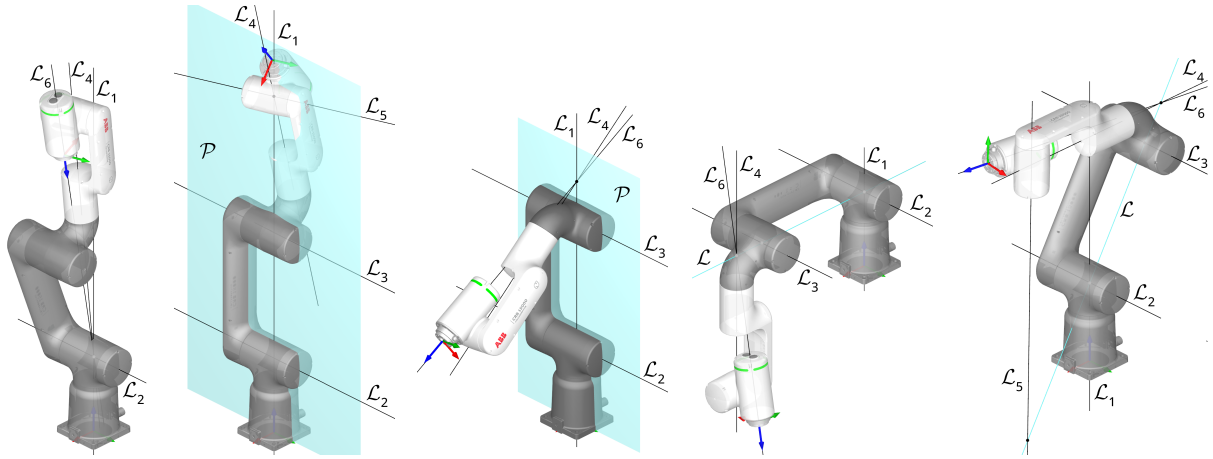

(h) case C_1 (i) case D_1 (j) case D_2 (k) case D_2' (l) case E_1

Fig. 3: Geometric interpretation of each type of kinematic singularity present in GoFa 5

TABLE III: Simplified, sufficient conditions for avoiding singularities in GoFa 5 (at least in theory)

Simplified conditions to avoid	Possible singularities
$\theta_2 = 0°$ or $180°$	D_1 and D_2
$\theta_3 = -104.34°$	A_1 and C_1
$\theta_4 = 0°$ or $\pm 90°$ or $180°$	A_2, B_1, B_2, B_2', B_3, B_4, D_2', and E_1

Category A: Two-screw dependency

Two screws can be dependent only when the joint axes are coincident. For GoFa 5, such configurations are only possible for the axes $\mathcal{L}_1$ and $\mathcal{L}_4$, and for $\mathcal{L}_1$ and $\mathcal{L}_6$.

A_1: $\mathcal{L}_1$ and $\mathcal{L}_4$ are coincident when $\theta_2 = 14.34°$ or $-165.66°$ and $\theta_3 = -104.34°$ (Fig. 3a). In $\mathcal{Q}'$, the singularity corresponds to two planes with an area of 78.96 rad^2.

A_2: $\mathcal{L}_1$ and $\mathcal{L}_6$ are coincident (Fig. 3b) when θ_2, θ_3, θ_4, and θ_5 satisfy one of the following two systems:

$$\begin{cases} \theta_4 = 0° \\ \pm\, a_5 + a_3\, s_{23} + a_2\, s_2 + d_4\, c_{23} = 0 \\ \theta_5 = \pm 90° - \theta_3 - \theta_2 \end{cases} \tag{9}$$

$$\begin{cases} \theta_4 = 180° \\ \pm\, a_5 + a_3\, s_{23} + a_2\, s_2 + d_4\, c_{23} = 0 \\ \theta_5 = \pm 90° + \theta_3 + \theta_2 \end{cases} \tag{10}$$

In $\mathcal{Q}'$, the singularity corresponds to four curves with a total length of 50.73 rad.

In GoFa 10 and 12, $\mathcal{L}_1$ and $\mathcal{L}_5$ can coincide too.

Category B: Three-screw dependency

In GoFa 5, there are only four sets of three screws that have a triple dependency.

B_1: $\mathcal{L}_1, \mathcal{L}_4$, and $\mathcal{L}_5$ are coplanar and concurrent (Fig. 3c) when $\theta_4 = \pm 90°$, and θ_2 and θ_3 satisfy the equation

$$d_4\, c_{23} + a_3\, s_{23} + a_2\, s_2 = 0. \tag{11}$$

In $\mathcal{Q}'$, the singularity corresponds to two surfaces, one for each value of θ_4, with a total area of 157.19 rad^2.

B_2: $\mathcal{L}_1, \mathcal{L}_4$, and $\mathcal{L}_6$ are coplanar and coincident (Fig. 3d) when $\theta_4 = 0°$ or $180°$ and when θ_2, θ_3, and θ_5 satisfy

$$a_5\, c_{23} + s_5\, (a_2\, s_2 + a_3\, s_{23} + d_4\, c_{23}) = 0. \tag{12}$$

In $\mathcal{Q}'$, the singularity corresponds to four surfaces with a total area of 276.38 rad^2.

B_2': $\mathcal{L}_1, \mathcal{L}_4$, and $\mathcal{L}_6$ are coplanar and parallel (Fig. 3e) when $\theta_2 + \theta_3 = \pm 90°$ or $270°$, $\theta_4 = 0°$ or $180°$, and $\theta_5 = 0°$ or $180°$. In $\mathcal{Q}'$, the singularity corresponds to eight lines with a total length of 61.21 rad.

B_3: $\mathcal{L}_2, \mathcal{L}_3$, and $\mathcal{L}_5$ are coplanar and parallel (Fig. 3f) when $\theta_3 = -76.83°$ and $\theta_4 = 0°$ or $180°$. In $\mathcal{Q}'$, the singularity corresponds to two planes with a total area of 78.96 rad^2.

B_4: $\mathcal{L}_2$, $\mathcal{L}_3$, and $\mathcal{L}_6$ are coplanar and parallel (Fig. 3g) when $\theta_3 = -74.25°$ or $-78.69°$, $\theta_4 = \pm 90$, and $\theta_5 = \pm 90$. In $\mathcal{Q}'$, the singularity corresponds to four lines with a total length of 25.13 rad.

In GoFa 10, $\mathcal{L}_2$, $\mathcal{L}_4$, $\mathcal{L}_6$ can be coplanar and concurrent too.

Category C: Four-screw dependency

In GoFa 5, there is only one case of four-screw dependency.

C_1: $\mathcal{L}_1$, $\mathcal{L}_2$, $\mathcal{L}_4$, and $\mathcal{L}_6$ are concurrent (Fig. 3h) when $\theta_3 = -104.34°$ and $\theta_5 = -174.90°$ or $5.10°$. In $\mathcal{Q}'$, the singularity corresponds to two planes with a total area of 78.96 rad^2.

In GoFa 10, the above singularity does not exist, since there is an offset between the axes of joints 1 and 2. However, there are two other four-screw dependencies.

- $\mathcal{L}_2$ and $\mathcal{L}_3$ lie in one plane, $\mathcal{L}_1$ and $\mathcal{L}_6$ lie in another. The two planes intersect at a common line, which passes through the intersection point of $\mathcal{L}_1$ and $\mathcal{L}_6$.
- $\mathcal{L}_2$ and $\mathcal{L}_3$ lie in one plane, $\mathcal{L}_4$ and $\mathcal{L}_6$ lie in another. The two planes intersect at a common line, which passes through the intersection point of $\mathcal{L}_4$ and $\mathcal{L}_6$.

Category D: Five-screw dependency

In GoFa 5, there are only two five-screw dependencies.

D_1: $\mathcal{L}_1$, $\mathcal{L}_2$, $\mathcal{L}_3$ lie in one plane, $\mathcal{P}$, and $\mathcal{L}_4$ and $\mathcal{L}_5$ intersect at a point in that plane (Fig. 3i) when $\theta_2 = 0°$ or $180°$ and $\theta_3 = -76.83°$. In $\mathcal{Q}'$, the singularity corresponds to two planes of a total area of 78.96 rad^2.

D_2: $\mathcal{L}_1$, $\mathcal{L}_2$, $\mathcal{L}_3$ lie in one plane, $\mathcal{P}$, and $\mathcal{L}_4$ and $\mathcal{L}_6$ intersect at a point in that plane (Fig. 3j) when $\theta_2 = 0°$ or $180°$, and θ_3 and θ_5 satisfy the following equation:

$$a_5\, c_3 + s_5\, (d_4\, c_3 + a_3\, s_3) = 0. \tag{13}$$

In $\mathcal{Q}'$, the singularity corresponds to two surfaces with a total area of 198.67 rad^2.

D_2': $\mathcal{L}_1$, $\mathcal{L}_2$, $\mathcal{L}_3$, $\mathcal{L}_4$, and $\mathcal{L}_6$ can also be normal to a common line, $\mathcal{L}$, and intersect it (Fig. 3k). This occurs when $\theta_2 = \pm 90°, \theta_3 = 0°$ or $180°$, $\theta_4 = \pm 90°$, and $\theta_5 = -170.20°$ or $-9.80°$. In $\mathcal{Q}'$, the singularity corresponds to 16 points.

In GoFa 10 and 12, the five-screw dependencies are the same.

Category E: Six-screw dependency

In GoFa 5, it is possible that all six screws are dependent, without any subset of them being dependent.

E_1: $\mathcal{L}_1, \mathcal{L}_2, \mathcal{L}_3, \mathcal{L}_4, \mathcal{L}_5$, and $\mathcal{L}_6$ are intersecting a common line $\mathcal{L}$ (Fig. 3l) when $\theta_4 = \pm 90°$ and θ_3 and θ_5 satisfy Eq. (13). In $\mathcal{Q}'$, the singularity corresponds to four surfaces with a total area of 397.32 rad^2.

A similar six-screw dependency exists in GoFa 10 and 12.

Summary

As we saw, none of the twelve different singularities in GoFa 5 is simple enough to describe in the robot's user manual. There are, however, several common joint-value conditions that are present in these singularities, and we have colored these joint values in Table II. These conditions, summarized in Table III, are sufficient, though conservative,

to avoid all singularities. The conditions are only slightly more complicated than the ones used by ABB in the YuMi cobot in order to avoid having too many exact but complex conditions for singularities [11].

V. Validation on the actual GoFa 5

The behavior of the real GoFa 5 near or at its singularities described in the previous section differs from that observed on conventional ABB robots. Beyond the standard "Close to singularity" message, the controller can produce other error messages, such as "Robot configuration error", "Geometric interpolation failed", and "Kinematic limitation", which cause the robot to stop at configurations whose joint angles deviate substantially from those listed in Table III. Conversely, the robot is sometimes able to cross singularities along certain Cartesian paths.

As noted above, a major issue in the current GoFa controller is that it rejects 8 of the 16 inverse-kinematic solutions. Indeed, the controller encodes configurations using the same scheme as spherical-wrist robots, a choice that likely contributes to the observed inconsistencies.

Accordingly, in the next section, although we will refer to commercially available robot arms, we restrict the study to their kinematic models and do not consider controller implementations. In other words, even if two of the cobots are equally "close" to a singularity, however that proximity is measured, one may refuse to move in Cartesian mode while the other does not.

VI. Comparison with A0509 and UR5e

Once all singularities of the GoFa 5 robot have been identified and described in the joint sub-space $\mathcal{Q}'$, it becomes possible to compare the proportion of singularities for each of the robots shown in Fig. 1. The singularities of the A0509 and the UR5 have already been described in [9], [21] and [10]; therefore, we will focus solely on deriving the corresponding expressions in the joint space. Recent studies comparing robot morphologies [22] highlight the importance of architecture in evaluating robot performance, which motivates our study.

Doosan's A0509

For Doosan's A0509, we follow the same procedure as described in Section III and obtain the following determinant, where the DH parameters are provided in Table IV:

$$\det(\mathbf{J}_{\text{A0509}}) = a_2 d_4 s_3 s_5 (d_4 s_{23} + a_2 s_2). \tag{14}$$

In the A0509, joints 2, 4, and 5 are restricted to $\pm 360°$, while joint 3 is restricted to $\pm 160°$. To evaluate and compare the results fairly, we reduce the range of joints 2, 4, and 5 to the half-open range $(-180°, 180°]$ and the range of joint 3 to $\pm 155°$, which results in the same joint travels as in GoFa.

The determinant in joint space leads to three distinct singularity conditions. Once again, these conditions are the minimal requirements for a singularity to occur (Table V).

TABLE IV: DH parameters of Doosan's A0509

i	θ_i	d_i (mm)	a_i (mm)	α_i
1	θ_1	155.5	0	$-90°$
2	$\theta_2 - 90°$	0	409	$0°$
3	$\theta_3 - 90°$	0	0	$-90°$
4	θ_4	367	0	$-90°$
5	θ_5	0	0	$90°$
6	$\theta_6 - 180°$	124	0	$0°$

TABLE V: Singularities of Doosan's A0509

Case	Axes	Condition
A_1	$\mathcal{L}_4, \mathcal{L}_6$	$\mathcal{L}_4 \equiv \mathcal{L}_6$
C_1	$\mathcal{L}_1, \mathcal{L}_4, \mathcal{L}_5, \mathcal{L}_6$	
E_1	$\mathcal{L}_1, \mathcal{L}_2, \mathcal{L}_3, \mathcal{L}_4, \mathcal{L}_5, \mathcal{L}_6$	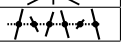

A_1: The so-called wrist singularity occurs when $\theta_5 = 0°$ or $180°$, resulting in two cubic singular regions with a total volume of 427 rad^3.

C_1: The shoulder singularity arises when the wrist center lies on the axis of joint 1. It is defined with the following equation, representing a curve of length 8.4 rad:

$$d_4 s_{23} + a_2 s_2 = 0. \tag{15}$$

E_1: Finally, the elbow singularity occurs when $\theta_3 = 0°$. Here, the line passing through the wrist center and the intersection of the axes of joints 1 and 2 also intersects the axis of joint 3. This condition results in one cubic singular region with a volume of 248 rad^3.

Universal Robots' UR5e

We apply exactly the same procedure to the UR5e and obtain the following determinant, where the DH parameters are provided in Table VI:

$$\det(\mathbf{J}_{\text{UR5e}}) = a_2 a_3 s_3 s_5 (a_2 c_2 + a_3 c_{23} - d_5 s_{234}) \tag{16}$$

TABLE VI: DH parameters of Universal Robots' UR5e

i	θ_i	d_i (mm)	a_i (mm)	α_i
1	θ_1	162.5	0	$90°$
2	θ_2	0	-425	$0°$
3	θ_3	0	-392.2	$0°$
4	θ_4	133.3	0	$90°$
5	θ_5	99.7	0	$-90°$
6	θ_6	99.6	0	$0°$

Again, for a fair comparison, although every joint of the UR5e is specified to rotate $\pm 360°$, we restrict joints 2, 4, and 5 to the half-open range $(-180°, 180°]$ and joint 3 to $\pm 155°$ (joint 3 is practically limited to about $\pm 165°$ anyway, due to self-collisions).

The determinant in joint space leads to three distinct singularity conditions, listed below and in Table VII.

TABLE VII: Singularities of UR5e

Case	Axes	Condition
B_1	$\mathcal{L}_2, \mathcal{L}_3, \mathcal{L}_4$	
C_1	$\mathcal{L}_2, \mathcal{L}_3, \mathcal{L}_4, \mathcal{L}_6$	
E_1	$\mathcal{L}_1, \mathcal{L}_2, \mathcal{L}_3, \mathcal{L}_4, \mathcal{L}_5, \mathcal{L}_6$	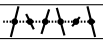

B_1: In this elbow singularity, we have the axes of joints 2, 3, and 4 parallel and in one plane. This singularity occurs when $\theta_3 = 0°$, resulting in one cubic singular region with a total volume of 248 rad^3.

C_1: In the wrist singularity, $\mathcal{L}_2$, $\mathcal{L}_3$, $\mathcal{L}_4$, and $\mathcal{L}_5$ are parallel, which occurs when $\theta_5 = 0°$ or $180°$, yielding two cubic singular regions with a total volume of 427 rad^3.

E_1: Finally, in the shoulder singularity, the intersection point of $\mathcal{L}_5$ and $\mathcal{L}_6$ lies in the plane spanned by $\mathcal{L}_1$ and $\mathcal{L}_2$. In terms of Grassmann line geometry, we have a degeneracy because a line parallel to $\mathcal{L}_2$ and passing through the intersection point of $\mathcal{L}_5$ and $\mathcal{L}_6$, also intersects $\mathcal{L}_1$, as well as $\mathcal{L}_2$, $\mathcal{L}_3$, and $\mathcal{L}_4$ at infinity. In the joint space, this singularity corresponds to a singularity surface of area 137 rad^2, defined by:

$$a_2 c_2 + a_3 c_{23} - d_5 s_{234} = 0. \tag{17}$$

ABB's GoFa 5

GoFa 5's singularity manifolds are shown in Fig. 4. In $\mathcal{Q}'$, there are 16 points, 16 curves of total length 137 rad, and 20 planes or surfaces of total area 1366 rad^2, and no volumes.

Do fewer singularities imply better dexterity?

Thus, GoFa 5 has fewer singular joint configurations than the UR5e and A0509. Among those fewer configurations, GoFa presents many different singularity types—twelve versus only three—but each GoFa type requires specific combinations of joint values, so individual singular configurations are relatively rare. By contrast, the UR5e and A0509 have singularities that occur when a single joint takes a specific value; such configurations occupy a larger portion of joint space and therefore arise much more frequently. That said, if ABB applied to GoFa the same singularity simplification strategy used in YuMi (the conditions in Table III), the cobot would be classified as having more singular joint configurations than the UR5e and A0509.

However, singular configurations are not the only concern; configurations that are near-singular are usually equally problematic. While various performance indices exist for identifying near-singular configurations [23], [24], none is perfect. Indeed, as noted by [24], most kinematic indices characterize the robot at a specific configuration and do not account for motion direction. Even at exact singular configurations, problems arise only for specific end-effector directions of motion on some industrial-robot brands (e.g., [25]). In what follows, we will use the manipulability index [26], aware of its limitations.

Comparison based on manipulability

Manipulability extends the concept of singularities by quantifying how freely the end-effector can move in different directions. As a configuration approaches a singularity, the manipulability decreases; at a singular configuration, it becomes null. The metric is the volume of the manipulability ellipsoid, which can be computed as [26]:

$$\mu = \sqrt{\det(\mathbf{J}\mathbf{J}^\top)}. \tag{18}$$

By substituting in the above formula the upper or lower 3×6 block of $\mathbf{J}$, we obtain the translation and orientation manipulability, respectively.

To ensure a fair manipulability comparison, we scaled down all GoFa link lengths by 10% and scaled up all Doosan A0509 link lengths by 6%, so that all three robots have the same maximum reach as the UR5e.

To evaluate and compare manipulability across the three resulting robots, we consider the Cartesian workspace relevant to a typical machine-tending operation, where the tool is a gripper mounted directly on the robot flange. Specifically, we consider a cube with a 600 mm side, discretized into 125,000 positions. At each position, four flange orientations are considered: facing front, down, right, and left. Then, at each pose, the inverse kinematics are solved to obtain all feasible joint configurations (up to 8 or 16).

First, we verified whether a standard machine-tending velocity was achievable given the maximum joint speeds: 250 mm/s along the end-effector z-axis, with a tolerance of 50 mm/s along the x and y axes and an orientation tolerance of $10°$/s. These motions were achievable at every pose within the workspace cube, with at least one joint configuration.

Then, for each pose, we computed the translation and orientation manipulability of the configuration that provides the highest manipulability. The statistical distribution across the Cartesian workspace of interest is shown in Fig. 5.

Thus, our results appear to confirm the common view that robots with offset wrists exhibit greater dexterity, especially in translation (e.g., [7], [8]). In practice, however, the joint configuration often needs to remain unchanged while following a Cartesian trajectory, for example during dispensing or welding. Further studies are therefore needed to evaluate manipulability under such constraints.

VII. Conclusions and Future Work

We analyzed the singularity structure of ABB's GoFa and compared it with two popular cobot architectures with simpler kinematics. Although the GoFa's singular configurations occupy a smaller fraction of joint space, they are more intricate to characterize and fall into 12 types, compared with three in the other two architectures. To simplify singularity avoidance in practice, we derived straightforward sufficient (though conservative) conditions. However, enforcing these conditions removes the advantage of the GoFa having fewer joint configurations to avoid.

In addition, while our preliminary study appears to confirm the prevailing view that robots such as the GoFa are more

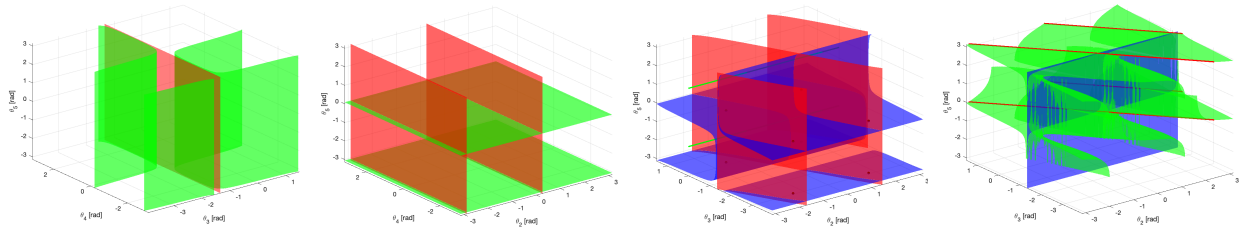

(a) $\theta_2 = 0°$ or $180°$ (b) $\theta_3 = -104.34°$ (c) $\theta_4 = \pm 90°$ (d) $\theta_4 = 0°$ or $180°$

Fig. 4: Overview of singularities in $\mathcal{Q}'$ subspace when one angle is fixed

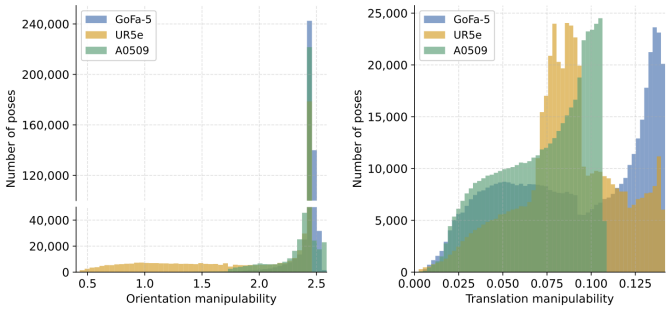

Fig. 5: Manipulability across specified Cartesian workspace

dexterous—at least for pick-and-place operations where the "best" configuration can be selected—further studies are needed to determine whether this advantage remains in path-following operations. Moreover, in such operations one must also account for the limitations of the GoFa controller, which allows only half of the up to 16 possible configurations.

While our study is not exhaustive, it contributes to the growing body of work questioning the practical advantages of such architectures.

Finally, the code developed in this paper is available here.

References

[1] K. H. Hunt, *Kinematic Geometry of Mechanisms*. Oxford: Clarendon Press, 1978.

[2] M. FarzanehKaloorazi, I. A. Bonev, and L. Birglen, "Simultaneous path placement and trajectory planning optimization for a redundant coordinated robotic workcell," *Mechanism and Machine Theory*, vol. 130, pp. 346–362, 2018.

[3] A. J. Elias and J. T. Wen, "Path planning and optimization for cuspidal 6R manipulators," 2025. [Online]. Available: https://arxiv.org/abs/2501.18505

[4] M. Lai, K. Go, Z. Li, T. Kröger, S. Schaal, K. Allen, and J. Scholz, "RoboBallet: Planning for multirobot reaching with graph neural networks and reinforcement learning," *Science Robotics*, vol. 10, no. 106, p. eads1204, 2025. [Online]. Available: https://www.science.org/doi/abs/10.1126/scirobotics.ads1204

[5] D. Pieper, "The kinematics of manipulators under computer control," Ph.D. dissertation, Stanford University, 1969.

[6] W. Shanda, L. Xiao, L. Qingsheng, and H. Baoling, "Existence conditions and general solutions of closed-form inverse kinematics for revolute serial robots," *Applied Sciences*, vol. 9, no. 20, 2019.

[7] L. Carbonari, M.-C. Palpacelli, and M. Callegari, "Inverse kinematics of a class of 6R collaborative robots with non-spherical wrist," *Robotics*, vol. 12, no. 2, p. 36, 2023.

[8] C. Trinh, D. Zlatanov, M. Zoppi, and R. Molfino, "A geometrical approach to the inverse kinematics of 6R serial robots with offset wrists," vol. 5C: 39th Mechanisms and Robotics Conference, p. V05CT08A016, 08 2015.

[9] M. J. D. Hayes, M. L. Husty, and P. J. Zsombor-Murray, "Singular configurations of wrist-partitioned 6R serial robots: a geometric perspective for users," *Transactions of the Canadian Society for Mechanical Engineering*, vol. 26, no. 1, pp. 41–55, 2002.

[10] M. H. FarzanehKaloorazi and I. A. Bonev, "Singularities of the typical collaborative robot arm," in *Volume 5B: 42nd Mechanisms and Robotics Conference, ASME 2018 International Design Engineering Technical Conferences and Computers and Information in Engineering Conference (IDETC/CIE)*, 2018.

[11] M. Asgari, I. A. Bonev, and C. Gosselin, "Singularities of ABB's YuMi 7-DOF robot arm," *Mechanism and Machine Theory*, vol. 205, p. 105884, 2025.

[12] ——, "Singularity analysis of Kinova's Link 6 robot arm via Grassmann line geometry," in *2024 IEEE International Conference on Robotics and Automation (ICRA)*. Yokohama, Japan: IEEE, 2024, pp. 8814–8820.

[13] D. H. Salunkhe, T. Marauli, A. Müller, D. Chablat, and P. Wenger, "Kinematic issues in 6R cuspidal robots, guidelines for path planning and deciding cuspidality," *The International Journal of Robotics Research*, vol. 44, no. 6, pp. 1035–1054, 2025.

[14] K. J. Waldron, S.-L. Wang, and S. J. Bolin, "A Study of the Jacobian matrix of serial manipulators," *Journal of Mechanisms, Transmissions, and Automation in Design*, vol. 107, no. 2, pp. 230–237, 1985.

[15] K. M. Lynch and F. C. Park, *Modern robotics: Mechanics, planning, and control*. Cambridge University Press, 2017.

[16] J.-P. Merlet, "Singular configurations of parallel manipulators and Grassmann geometry," *The International Journal of Robotics Research*, vol. 8, no. 5, pp. 45–56, 1989.

[17] I. Zaplana, H. Hadfield, and J. Lasenby, "Singularities of serial robots: Identification and distance computation using geometric algebra," *CoRR*, vol. abs/2109.12470, 2021.

[18] D. Calzolari, R. Lampariello, and A. M. Giordano, "Singularity maps of space robots and their application to gradient-based trajectory Planning," in *Proceedings of Robotics: Science and Systems*, 2020.

[19] H. Grassmann, *Die Ausdehnungslehre: Vollständig und in strenger Form bearbeitet*, ser. Cambridge Library Collection - Mathematics. Cambridge University Press, October 2013, reprint of the original.

[20] F. Hao and J. M. McCarthy, "Conditions for line-based singularities in spatial platform manipulators," *Journal of Robotic Systems*, vol. 15, no. 1, pp. 43–55, 1998.

[21] M. Weyrer, M. Brandstötter, and M. Husty, "Singularity avoidance control of a non-holonomic mobile manipulator for intuitive hand guidance," *Robotics*, vol. 8, no. 1, 2019.

[22] N. Gautier, Y. Guillermit, Y. Sebsadji, M. Porez, and D. Chablat, "Comparison of robot morphologies and base positioning for welding applications," in *Proceedings of the ASME 2024 International Design Engineering Technical Conferences and Computers and Information in Engineering Conference (IDETC-CIE)*, vol. 7, 2024.

[23] P. Cardou, S. Bouchard, and C. Gosselin, "Kinematic-sensitivity indices for dimensionally nonhomogeneous Jacobian matrices," *IEEE Transactions on Robotics*, vol. 26, no. 1, pp. 166–173, 2010.

[24] G. Boschetti and T. Sinico, "Performance comparison of two architectures of 6R articulated robots," *Machines*, vol. 11, no. 2, 2023.

[25] Mecademic, "Crossing singularities with a six-axis industrial robot arm," YouTube, [Online; accessed 5-Sep-2025]. [Online]. Available: https://youtu.be/MA_tsx0i6DM

[26] T. Yoshikawa, "Dynamic manipulability of robot manipulators," *Transactions of the Society of Instrument and Control Engineers*, vol. 21, no. 9, pp. 970–975, 1985.